Journal of Alloys and Compounds 523 (2012) 11–15

Contents lists available at SciVerse ScienceDirect

Journal of Alloys and Compounds

journal homepage: www.elsevier.com/locate/jallcom

Characterization of 3R martensite in a Ni–40Al–15Pt bulk alloy

Marie Clancy[a,*], Michael J. Pomeroy[a,b], Calum Dickinson[b]

[a] Department of Materials Science and Technology, University of Limerick, Castletroy, Ireland
[b] Materials and Surface Science Institute, University of Limerick, Castletroy, Ireland

ARTICLE INFO

Article history:
Received 1 November 2011
Received in revised form 23 January 2012
Accepted 24 January 2012
Available online 13 February 2012

Keywords:
NiAlPt
Martensite
Twinning
FIB milling
TEM

ABSTRACT

As Pt promotes the reversible martensite transformation, the aim of this study was to assess the influence of Pt on the crystallography of (β′) martensite, in terms of ordering adapted, twinning and stacking faults. The focused ion beam (FIB) milling process was used to prepare transmission electron microscopy (TEM) samples of the NiAlPt bulk alloys, whereby 3R, $L1_0$ ordering of the martensite was confirmed. The addition of Pt, coupled with high temperature oxidation resulted in more stacking faults, due to greater Pt diffusion and subsequent enrichment in martensite. For Pt diffusion the temperature must be in excess of 900 °C, both for isothermal and cyclic oxidation. When the favorable temperature environment is achieved Pt can diffuse preferentially allowing for promotion of the transformation to martensite.

1. Introduction

The intermetallic β-NiAl compound offers excellent strength at high temperatures, good oxidation resistance and high thermal conductivity [1]. The phase's resistance to high temperature oxidation makes it particularly suitable for applications in the gas turbine industry, where turbines are subjected to thermal cycling at temperatures in excess of 900 °C. Fortunately, the β-NiAl phase represents a large area of the Ni–Al phase diagram [2]. Rosen and Goebel introduced the needle-like martensite structure Ni_xAl_y, describing it as a structure with $L1_0$ ordering that is derived from the parent NiAl CsCl structure on quenching [3]. Martensite corresponds to the $AuCu_1$ structure so it is described as FCT. Martensite may occur in the ~61–69 at.% Ni region of the Ni–Al phase diagram [2] and it does so by a reversible diffusionless transformation, where the atoms are displaced and the ordered cubic parent structure becomes distorted. The level of tetragonality is due to the spacing of pure Ni and mixed NiAl planes in the ⟨0 0 1⟩ direction and as the Ni content rises excess Ni atoms are accommodated on the (0 0 1) face centers. Pt is a popular addition to NiAl alloys as it partitions preferentially to the β phase where it has a good solubility, thus widening the β phase field [4]. The presence of Pt in the alloy aids in the preferential transformation of β-NiAl to ductile β′-martensite instead of brittle γ′-Ni_3Al. In the NiAlPt system, the martensitic transformation is encouraged by Pt's preferential substitution for Ni.

This paper illustrates what effect Pt has, if any, on the crystallography of the martensite formed on quenching. It is the objective of this paper to assess if Pt alters the chemistry of the martensite formed on quenching, and how significantly does this differ from the parent β-NiAl phase from which it is derived.

2. Martensite in NiAl

2.1. Martensite growth

A variety of factors control the rate at which martensite grows, the type that forms and at what temperature it will occur. These include: the degree of ordering of the crystal lattices, the number of defects, the defect types (ordered or disordered faults, twinning, vacancies and dislocations) and the local stress configurations [5]. Refinement of the parent phase can make it difficult for martensite to nucleate and this is also the case if the alloy has been subjected to solid-solution strengthening, as this would account for improved resistance to dislocation type motion [6].

Increasing the Ni level decreases β stability by reducing ordering forces between Ni and Al. Therefore, as β′ is less shear resistant it requires less energy for it to manifest. The development of martensite in a β-faulted region requires that martensite may propagate by dislocation motion, which is typically thermally activated. Martensite originates by the movement of atoms over distances that are less than the inter-atomic spacing. The atoms move by breaking inter-atomic bonds and then making new bonds [4,7].

* Corresponding author at: ARC CoE – Light Metals, Monash University, Clayton, VIC 3800, Melbourne, Australia. Tel.: +61 399051928; fax: +61 399054940.
E-mail address: marie.clancy@monash.edu (M. Clancy).

0925-8388/$ – see front matter © 2012 Elsevier B.V. All rights reserved.
doi:10.1016/j.jallcom.2012.01.129

2.2. Martensite twinning

Twinning is attributed to the displacement of atoms on one side of a plane, while the other side is a mirror image [8]. Twinning occurs on specific crystallographic planes and in directions that are dependent on the crystal structure. Twinning and any subsequent de-twinning are methods of ensuring an undistorted habit plane [9]. As the habit plane remains unchanged by not deforming or rotating it stays directly related to the close packed plane [10] and so the twins arrange themselves relative to one another on the habit plane. Close packed planes with planar defects act as good glide planes for interface dislocations. If these defects are not present however, the planes cannot act as glide paths until later in the process [11].

Enami identified martensite as a "striated" structure that had internal twins prominent on the (1 1 1) plane in the ⟨1 1 2⟩ direction [12]. The β′ laths are related to each other by a rotation of 60° around the normal to the close packed (1 1 0) planes, which gives a twin relationship of (1 1 2) between two laths. Chen and Han agreed almost fully with this relationship, saying that the twin system lies on $(1\,1\,1)/<1\,1\,\bar{2}>$ [13]. Litvinov stated that β′ needles are in twin orientation with twinning planes of the (1 0 0) family [14] and ordering was noted as continuous over the β′ interfaces [15].

The width of micro-twins can vary and their presence is indicated by streaking in the DP (diffraction pattern). The micro-twin planes of the β′ structure accommodate the constant shear of the transformation, i.e. the habit plane stress, which exists because the parent material, NiAl, has a small twin surface energy [15]. The plate widths of the martensite needles were found to be as thin as 6.6 nm [11] and the stacking sequence of β′ in β was found to vary quite considerably, with wide twins of up to several hundred nanometers often observed. Stress or change in temperature can cause de-twinning, allowing the atoms to re-arrange themselves more efficiently in the new environment.

2.3. Crystallography of martensite

Some martensitic structures are more stable than others, depending on their composition. In the NiAlPt system there are two main types of martensite which can occur; 2 M (3R) and 14 M (7R). The 3R ordering is adapted when the Al content is less than 37 at.% [16]. Even if the martensite structure changes from 3R to 14 M, the shear and habit planes will not alter to any great extent [17]. The 3R martensitic ordering offers high thermal conductivity, high temperature strength and excellent oxidation and corrosion resistance [18]. This structure is highly symmetrical [19] with long period stacking order [20]. The high symmetry lends itself to less strain contrast with the β matrix [11] and so the 3R configuration is more prevalent as it is easy for the parent phase to accommodate it. 3R martensite is a long period structure with complex periodic stacking faults [21]. Short range ordering may be achieved in this structure by vacancy diffusion and it is a means of stabilizing the martensite structure [22]. This decreases the amount of free energy by increasing the number of nearest unlike pairs of atoms, e.g. (A–B) [23]. The stacking sequence of β′, which is based on the martensite basal plane, corresponds to the $(1\,1\,0)_{\beta}$ plane. This gives a periodic stacking of ABC–ABC–ABC, whereby A, B and C represent three different orderings of atoms [24].

The stress at the habit plane is accommodated by fine micro-twinning on the Face Centred Tetragonal $\{1\,1\,1\}_{FCT}$ planes [11], which is possible due to the twin surface energy being quite small. Fringes that are visible in micrographs of the 3R β′ structure may be attributed to the overlapping stacking faults which have undergone an increase in numbers. There are alternating sequences of martensite stacking's and these have a stepped interface.

Table 1
Heat treatment history of the NiAlPt alloys.

Alloy #	Condition
1	Oxidized for 100 cycles in air, between 750 °C (1 min hold) and 1150 °C (1 h hold). A ramp rate of 15 °C/min was used before cooling from 750 °C at a rate of 15 °C/min.
2	Oxidized for 100 cycles in air, between 950 °C (1 min hold) and 1150 °C (1 h hold). A ramp rate of 15 °C/min was used before cooling from 950 °C at a rate of 15 °C/min.
3	Oxidized for 5 h at 1000 °C before sealing in quartz, under Ar for 100 cycles between 750 °C (1 min hold) and 1150 °C (1 h hold). A ramp rate of 20 °C/min was used before cooling from 750 °C at a rate of 15 °C/min.

3. Experimental methods

The Ni–40Al–15Pt alloys were provided by the AMES Laboratory, Iowa State University in three different conditions, as presented in Table 1.

An FEIFIB 200 operated at 30 keV was used to prepare foils for TEM analysis and these were milled at 90° to the oxide surface of the alloy. TEM imaging and diffraction was conducted on a JEOL JEM-2011 microscope with a LaB_6 filament, at an accelerating voltage of 200 keV. Energy dispersive X-ray spectroscopy (EDS) and high-angle annular dark-field (HAADF) analysis were performed using the JEOL FEG2100F TEM, also operating at 200 keV.

4. Results and discussion

4.1. Crystallography of martensite

The martensite microstructure is shown in Fig. 1(a) and (b). Fig. 2 shows an indexed DPof the identified 3R martensite structure, with twinning of the (1 1 1) and (2 0 0) planes. All of the images in Figs. 1 and 2 are of the alloy that was cyclically oxidized at 950 °C. The weaker spots are actually the superstructure reflections and the presence of three of these in each sequence confirms the 3R martensitic structure.

All of the alloys produced martensite and there were no distinctive differences between the martensite formed in each alloy, except the alloy that was cycled at the higher temperature of 950 °C showed evidence of finer micro-twinning. Fig. 1(a) shows martensite needles of approximately 0.3 μm width that are embedded in the β matrix. The width of the martensite needles varied within each alloy and so there was no obvious effect of different cycling temperatures in this respect except that the very narrow micro-twins as shown in Fig. 1(b) were only found in the alloy that had been cycled between 950 °C and 1100 °C. These finer twins, measuring ~8 nm are indicative of more stacking faults in the structure and their presence suggests that the martensite in this instance had to accommodate more internal stress at the higher temperature. The high internal stress in this alloy could be related to the enhanced diffusion of Pt at higher temperatures, and the resultant strain that the martensite incurred owing to the increased Pt concentration in the lattice.

There is evidence of twinning and internal micro-twinning in all three of the alloys. Internal micro-twinning is a means of accommodating the lattice strains while minimizing the stress for each particular β/β′ configuration. Twinning is encouraged by the rapid quenching or application of stress, both of which induce the martensite. Twinning is a positive process as it allows the atoms to arrange themselves in strain-accommodating manners which can enhance cohesion while reducing misfit [23].

A representative area of the fine micro-twins is shown in Fig. 2(a) with the accompanying diffraction pattern, in Fig. 2(b). The latter of these was indexed as being the (1 1 1) and (2 0 0) planes, which are members of the $[0\,\bar{1}\,1]$ zone axis, with an angle of 56.7° between them. The twin systems are indexed and highlighted in contrasting

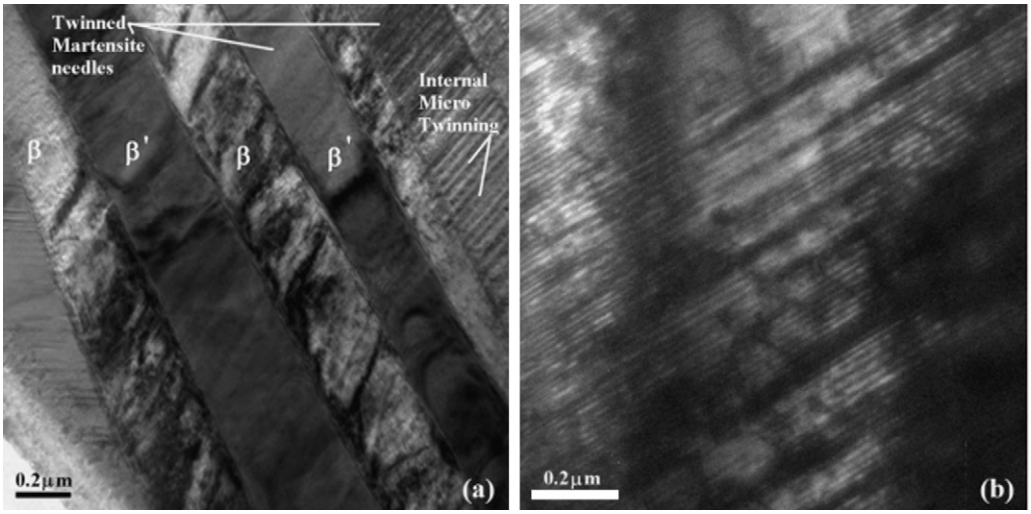

Fig. 1. Martensite microstructure inNi–40Al–15Pt.

colors in Fig. 1(c). As the twins become thinner and their density increases, it becomes increasingly difficult to obtain a DP that shows the super-lattice orientation of the twins. This is not due to any other ordering of the martensite occurring, it is simply due to the twinning effect causing streaking within the DP [24].

High temperature oxidation caused the Al content of the alloy to drop to a level, such that 3R ordering was adopted by the martensite [26]. As Pt preferentially substitutes for Ni, the critical Al limit for 3R ordering was not influenced by the presence of Pt. The martensite ordering was confirmed by diffraction analysis, as shown in Fig. 2, and by comparison with others [5,25]. To confirm the presence of 3R the weak beam spots were studied using the twin-defect DP in Fig. 2(b). Twinning distorts the DP and so it can be difficult to interpret the weak beam spots that identify the 3R stacking order. As previously outlined, the ordering of the martensite depends on the chemistry of the alloy and, in this instance, if the system has less than 37 at.% Al then the 3R $L1_0$ structure is adopted.

4.2. Chemistry of the martensite needles

A series of STEM EDS point analyses were conducted on each of the three alloys to determine the chemistry of the matrix and the needles. The data points chosen from each of the alloys are shown in Fig. 3. The images displayed in Fig. 3 are compositional rather than topological representations of the three alloys and these images were captured at lower magnifications than what was used for Figs. 1 and 2, hence the apparent difference in morphologies and level of twinning. The computed compositional differences between the β matrix and the β′ needles are presented in Table 2. The percentage differences were calculated by subtracting the atomic per cent (Ni, Pt and Al) contents for the β-NiAl phase from

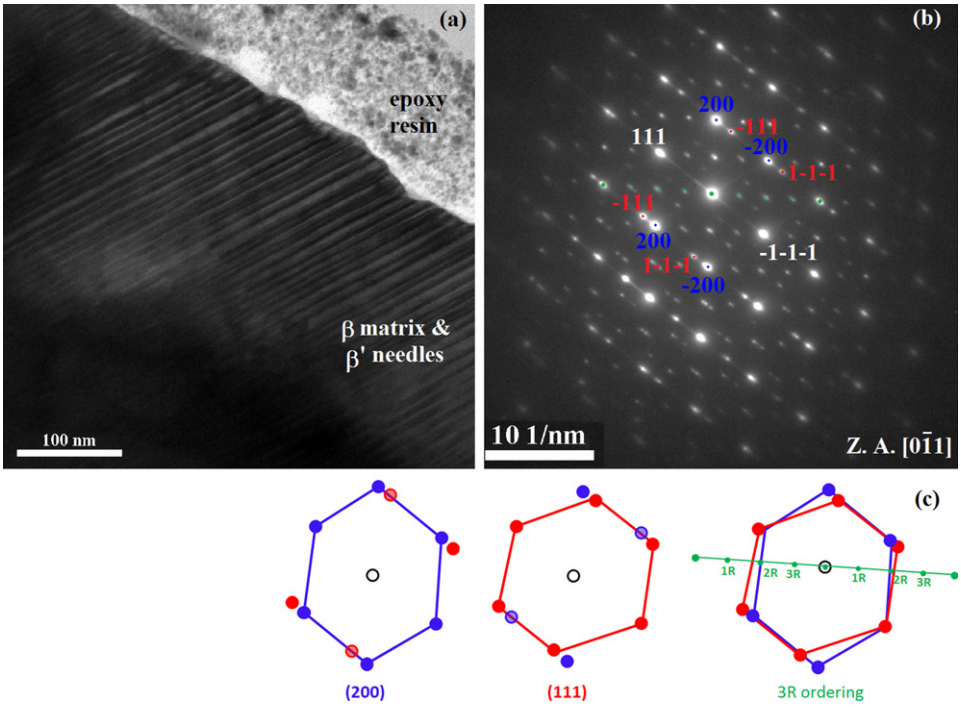

Fig. 2. (a) 3R martensite, (b) DP of [0 $\bar{1}$ 1] zone axis and (c) indexed twins on the $(1\,1\,1)_{red}$ and $(2\,0\,0)_{blue}$ planes with the identified 3R superstructure reflections$_{(green)}$.

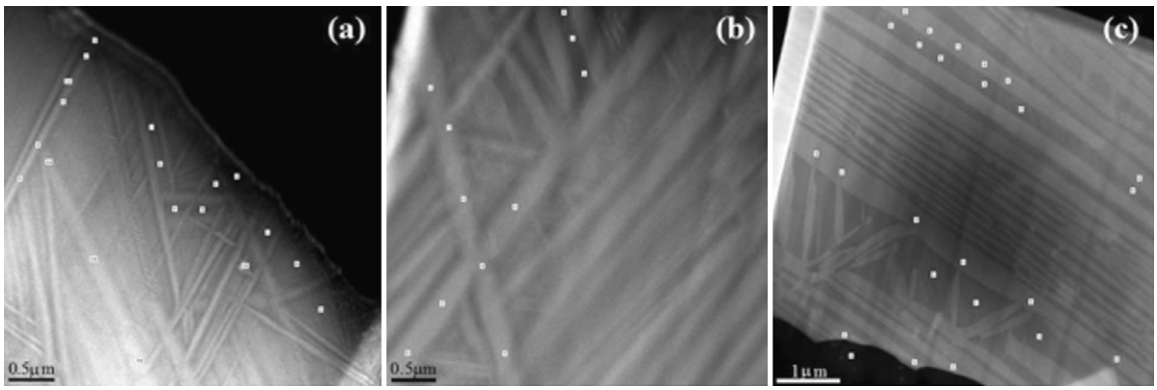

Fig. 3. HAADF images showing the points used for EDS mapping of the Ni–40Al–15Pt alloys after (a) oxidation between 750 °C and 1150 °C for 100 cycles (b) oxidation between 950 °C and 1150 °C for 100 cycles and (c) 5 h of isothermal oxidation at 1000 °C prior to 100 cycles of oxidation between 750 °C and 1150 °C.

the β′-martensite and then assessing the difference as a percentage, with respect to the composition of the martensite.

Fig. 3 shows qualitatively the difference in composition between the martensite needles and the untransformed parent β matrix, with the areas of brighter contrast representing the Pt rich needles embedded in the β matrix. There was no change in composition in different needles within any one of the foils; with respect to various sections within the needle itself, the needles proximity to the TGO/alloy interface and needle orientation. For that reason an average Ni, Pt and Al composition could be obtained for the martensitic needles and the β matrix in which the needles were embedded.

While martensite is only possible within a Ni range of 61–68 at.% for the binary Ni–Al system [3]. However Pt, by its ability to substitute for Ni, allows for this transformation to occur under Ni poor conditions. Prior to any thermal treatment, Ni and Pt collectively account for 60 at.% of this bulk alloy and considering that a percentage of Al diffused outward to grow a layer of alumina during the oxidation process, the alloy has a greater propensity to transform to martensite. It can be seen from the data presented in Table 2 that cycling the alloy to a lower temperature (750 °C) significantly reduced the diffusivity of Pt. The martensite needles formed contained only 3 at.% Pt enrichment (relative to the β matrix), in comparison to the needles formed in the alloy cycled between 950 °C and 1150 °C, which had 16 at.% enrichment. This is evidence that the favorable characteristics of Pt rely on very high temperature environments for them to be realized. For the same alloys, Ni enrichment in the martensitic needles was nearly four times higher in the alloy cycled at the higher temperature. Al depletion in the martensite was greater also for the alloy that was cycled between 950 °C and 1150 °C. This is a favorable occurrence as more Al is retained in the parent β-NiAl phase and so it is available for outward diffusion to the surface so that the protective overlying oxide layer can form. The alloy's provision of Al for the formation of the alumina oxide is critical so that the substrate (alloy) is exposed to the absolute temperatures for less time, as the ceramic oxide can absorb as much as 160 °C [2].

As Pt diffusion was proven to be a result of high temperature cyclic oxidation at 950 °C, it was of interest to know if this level of Pt diffusion could be enabled at lower temperatures. The alloy that had been subjected to five hours of oxidation at 1000 °C prior to thermal cycling from 750–1150 °C was shown to also allow for high levels of Pt diffusion. As outlined in Table 2, this alloy contained martensite needles that had levels of Pt 3% higher than those of the alloy which was subjected to cyclic oxidation at 950 °C, where there was a 19% difference between the Pt content of the martensite and the β-NiAl phase. This suggests that isothermal oxidation at an elevated temperature could be a useful pre-step for enhancing Pt diffusion in alloys that might not be operating at extremely high temperatures (over ~800 °C).

Table 2
Compositional difference (Δ) of the β′ needles, relative to the β matrix.

Composition	Alloy #	Δ % (Ni)	Δ % (Al)	Δ % (Pt)
Ni–40Al–15Pt	1	2.62	−4.22	3.03
	2	9.79	−19.96	16
	3	4.47	−13.92	18.9

5. Conclusions

- An increase in Pt diffusion activity prior to quenching will increase the likelihood of martensite forming on quenching.
- As Pt preferentially partitions to Ni sites, its presence does not alter the preferred ordering of the martensite, and it was confirmed to be 3R $L1_0$. The increased Pt content in the martensite resulted in very fine micro-twinning and this was evident by streaking in the DPs.
- Isothermal oxidation at 1000 °C, prior to cyclic oxidation enhances the diffusivity of Pt in martensite, while minimizing the diffusion of Ni and Al, in comparison to an alloy that had just been cycled to 950 °C.
- High temperature cycling between 950 °C and 1150 °C, allows for heightened level of diffusion, and this resulted in significant Pt and Ni enrichment of the martensite needles, as was expected. This higher temperature oxidation allowed for greater depletion of Al levels, as Al diffused outward to form the alumina layer.
- The presence of Pt will only have an impact on martensite when temperatures in excess of ~900 °C are used as it needs thermal activation for more pronounced diffusivity.

Acknowledgment

The authors would like to acknowledge Brian Gleeson, formerly of the Ames Laboratory at Iowa State University, for providing the alloys for this study.

References

[1] R.J. Thompson, J.C. Zhao, K.J. Hemker, Intermetallics 18 (May (5)) (2010) 796–802.
[2] J.H. Chen, J.A. Little, Surface and Coatings Technology 92 (1–2) (1997) 69–77.
[3] S. Rosen, J.A. Goebel, Transactions of the Metallurgical Society of AIME 242 (4) (1968) 722–724.
[4] M. Reid, PhD thesis, University of Limerick, 2002.
[5] D. Schryvers, D. Holland-Moritz, Materials Science and Engineering A 273 (275) (1999) 697–702.
[6] H.S. Yang, H.K.D.H. Bhadeshia, Scripta Materialia 60 (2009) 493–495.
[7] M.F. Ashby, D.R.H. Jones, Engineering Materials 2, Pergamon, 1986.

[8] P. Sittner, V. Novák, International Journal of Plasticity 16 (10–11) (2000) 1243–1268.
[9] M. Ahlers, Smart Materials and Structures 16 (2007) 115–125.
[10] E. Patoor, D.C. Lagoudas, P.B. Entchev, L. Catherine Brinson, X. Gao, Mechanics of Materials 38 (5–6) (2006) 391–429.
[11] D. Schryvers, Y. Ma, Materials Letters 23 (1–3) (1995) 105–111.
[12] K. Enami, S. Nenno, K. Shimizu, Transactions of the Japan Institute of Metals 14 (2) (1973) 161–165.
[13] L. Chen, Y. Han, Materials Science and Engineering A 329 (331) (2002) 725–728.
[14] V.S. Litvinov, I.N. Bogachev, A.A. Arkhange, E.G. Pantsyre, Fizika Metallov I Metallovedenie 36 (2) (1973) 388–393.
[15] D. Schryvers, Y. Ma, Journal of Alloys and Compounds 221 (1–2) (1995) 227–234.
[16] J. Lasek, T. Chraska, P. Krecek, P. Bartuska, Scripta Materialia 37 (6) (1997) 897–902.
[17] U.D. Hangen, G. Sauthoff, Intermetallics 7 (3–4) (1999) 501–510.
[18] H.J. Kang, S.K. Wu, L.M. Wu, Intermetallics 18 (1) (2010) 123–128.
[19] K. Otsuka, X. Ren, Materials Science and Engineering A 312 (1–2) (2001) 207–218.
[20] E. Artunç, Physica B: Condensed Matter 366 (1–4) (2005) 138–145.
[21] S. Kazanc, S. Ozgen, O. Adiguzel, Physica B: Condensed Matter 334 (3–4) (2003) 375–381.
[22] K. Marukawa, K. Tsuchiya, Scripta Metallurgica et Materialia 32 (1) (1995) 77–82.
[23] K. Otsuka, X. Ren, Materials Science and Engineering A 273 (275) (1999) 89–105.
[24] F.C. Levey, M.B. Cortie, Materials Science and Engineering A 303 (1–2) (2001) 1–10.
[25] M. Chandrasekaran, L. Delaey, Journal de Physique 43 (1982) 661.
[26] T. Czeppe, Materials Chemistry and Physics 81 (2–3) (2003) 463–465.